

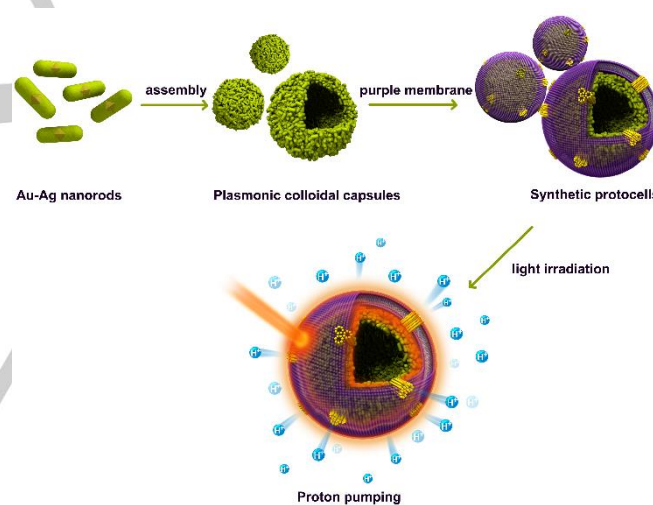
Light-Gated Synthetic Protocells for Plasmon-Enhanced Chemiosmotic Gradient Generation and Phosphorylation

Zhaowei Chen,^{[a],†} Gleiciani De Queiros Silveira,^{[a],†} Xuedan Ma,^[a] Yunsong Xie,^[b] Yimin A. Wu,^[a] Edward Barry,^[b] Tijana Rajh,^[a] H. Christopher Fry,^[a] Philip D. Laible,^[c] and Elena A. Rozhkova^{*,[a]}

Abstract: Here, we present construction of a light-gated synthetic protocell model made of plasmonic colloidal capsules (CCs) assembled with lipoprotein bacteriorhodopsin for converting solar energy into electrochemical gradients and further driving synthesis of energy storage molecules. Not only did this synthetic protocell incorporate essential features of CCs (such as compartmentalization and semipermeability), but it also assimilated such an important intrinsic property of noble metal colloidal particles as plasmonic resonance. Specially, the near-field coupling between adjacent metal nanoparticles gave rise to strongly localized electric fields and resulted in a broad absorption in the whole visible spectra, which in turn promoted the flux of photons to bacteriorhodopsin and accelerated the proton pumping kinetics. The cell-like potential of this design was further demonstrated by leveraging the outward pumped protons as 'chemical signals' for triggering ATP biosynthesis in a coexistent protocell population. Hereby, we lay the ground work for engineering of colloidal supraparticle-based protocells with higher-order functionalities.

Engineering of synthetic protocells (or artificial cells) with man-made compartments to reproduce specific cellular functions has received significant attention in fields ranging from origins-of-life research to synthetic biology and biomedical sciences.^[1] Usually, models of protocells are based on self-assembled vesicles comprising amphiphilic molecules since all present-day cells have lipid-defined membranes.^[2] Nonetheless, inspired by the hydrothermal-vent origin-of-life hypothesis that prebiotic syntheses were confined and catalyzed by compartment-like iron monosulfide precipitates,^[3] synthetic protocells constructed with inorganic nanoparticle-packed CCs (e.g. colloidosomes) have recently been put forward as an alternative primitive paradigm.^[4] The hallmark characteristics of CCs are their internal space, tunable semipermeability, and versatile choice of colloidal particle precursors with different functionalities.^[5] In this scenario, inorganic synthetic protocells capable of housing cell-free gene expression and enzyme catalysis,^[6] controlled release/uptake,^[7] growth and division,^[8] and inter-protocellular communication^[9] have been proposed. In these studies, colloidal particles were

primarily utilized as compartment boundaries, while the contribution of their physicochemical properties remain less discussed. On the other hand, along the line of hydrothermal origin hypothesis, an important evolution stage occurred when protocells simultaneously relied on inorganic walls and organic membranes to orchestrate protometabolic reactions, after which primordial membranes got off the ground and formed free-living cells.^[3b,3c] Natural questions that follows are whether and how the attributes of the inorganic matter might influence the biological processes of protocells during this process. In this context, protocell models constructed with CCs to mirror this phase would provide deep insights of the plausible roles which inorganic matter might play in the transition from geochemistry to biochemistry of early life, which at the same time also paves the way for developing new type of cell-mimic functional materials.



Scheme 1. Construction of light-gated synthetic protocells. Plasmonic colloidal capsules (CCs) are formed by self-assembly of Au-Ag nanorods; then, channel protein, bacteriorhodopsin (shown as trimers in yellow in the synthetic protocells), in the form of purple membranes, is fused over the surface of CCs to form isolated compartments, namely synthetic protocells. Upon light irradiation, both the photocycle of bacteriorhodopsin and the plasmonic field of the Au-Ag nanorods are excited. The near-field coupling between adjacent Au-Ag nanorods generate strong local plasmon field, which in turn accelerates the photocycle of bacteriorhodopsins and promotes the proton pumping kinetics.

In this study, we attempted to fill this gap by constructing a light-gated synthetic protocell based on plasmonic CCs that were assembled with bacteriorhodopsin for solar-driven proton gradient generation and communication-mediated ATP synthesis, with which we studied the effect of colloidal bricks' plasmon resonance on the performance of the cytomimetic system (**Scheme 1**). Bacteriorhodopsin, classified as the "other" photosynthetic system, exists as a lipoprotein complex arranged in a two-dimensional hexagonal lattice known as the purple

- [a] Dr. Z. Chen,[†] Dr. G. de Queiros Silveira,[†] Dr. X. Ma, Dr. Y. Wu, Dr. T. Rajh, Dr. H. C. Fry, Dr. E. A. Rozhkova
Center for Nanoscale Materials, Argonne National Laboratory,
Argonne, IL 60439, USA
E-mail: rozhkova@anl.gov
- [b] Dr. Y. Xie, Dr. E. Barry
Applied Materials Division, Argonne National Laboratory, Argonne,
IL 60439, USA
- [c] Dr. P. D. Laible
Biosciences Division, Argonne National Laboratory, Argonne, IL
60439, USA

[†]The authors contributed equally to this work.

Supporting information for this article is given via a link at the end of the document.

membrane (PM) of Archaea *Halobacterium salinarum*, and pumps protons unidirectionally from the cytoplasmic to the extracellular side via a series of photointermediates upon light adsorption (Figure S1).^[10] Herein, we first prepared robust plasmonic CCs via assembling Au-Ag nanorods (AuAgNRs) at water-in-oil Pickering emulsion interfaces. The obtained plasmonic CCs displayed intense broadband absorption in the whole visible range as a result of the strong interparticle near-field coupling in the shell. Bacteriorhodopsins in the form of PMs were then wrapped over the AuAgNR CCs via electrostatic interaction to create isolated compartments. As a result, a synthetic protocell that could steadily acidify the external medium under irradiation was established. Systematic study of the proton pumping kinetics suggested that the strong plasmonic field near the AuAgNR CC surface could concentrate photons around bacteriorhodopsin, thus accelerating their natural photocycle. By further coupling a second population of protocells containing ATP synthase molecular motors to this light-gated signaling pathway, an artificial synthetic community was established for driving ATP synthesis.

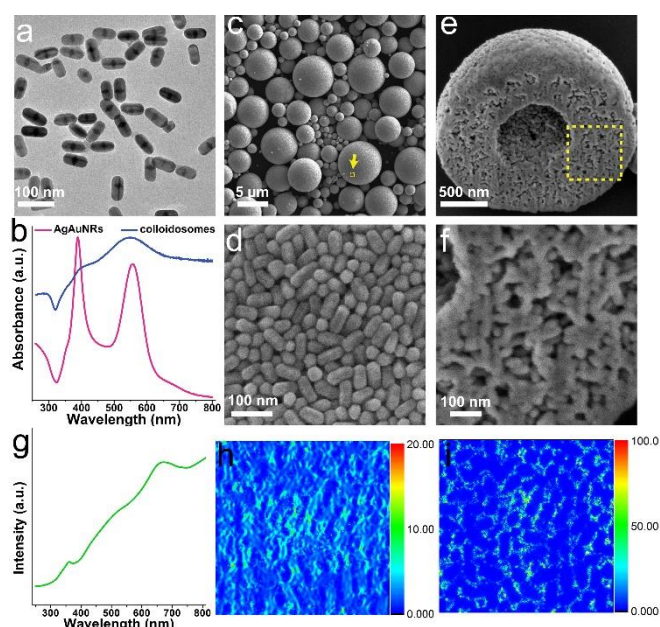


Figure 1. (a) Transmission electron microscopy image of AuAgNRs. (b) UV-Vis absorption spectrum of AuAgNRs and CCs. (c) SEM image of the plasmonic CCs. (d) High-magnification SEM image of the arrow-pointed frame in (c). (e) Focused ion beam (FIB)/SEM image of the milled CCs. (f) High-magnification FIB/SEM image of the frame in (e). (g) FDTD-simulated extinction spectrum of a real sample calculated from panel d and the corresponding $|E|^2$ distribution at 410 nm (h) and 570 nm (i).

To prepare plasmonic CCs, $\sim 64 \times 33$ nm Au-Ag heterogeneous nanorods (AuAgNRs) stabilized by positively charged ligand were first synthesized (Figure 1b, Figure S2-3). The two strong absorption peaks observed at 390 and 556 nm in the UV-Vis spectrum were attributed to the transverse and longitudinal localized surface plasmon resonances of AuAgNRs, respectively (Figure 1b). Then, by emulsifying an aqueous suspension of AuAgNRs (~ 5 wt%) with 1-butanol (1:10 by volume), water-in-1-butanol Pickering emulsions were initially

formed, driven by the reduction in interfacial free energy.^[11] Next, as the water in the discontinuous phase diffused into the 1-butanol phase,^[5c] the AuAgNRs packed together via van der Waals forces, forming closed CCs with dimensions ranging from several hundred nanometers to a few micrometers (Figure 1c, Figure S4). Close inspection of the CCs revealed a well-defined porous structure composed of randomly but densely packed AuAgNRs (Figure 1d). After further milling the CCs with focused ion beams, the hollow inner cavity and multilayer-stacked shells were clearly identified (Figure 1e, f). From the surface and the milled shell view, it could be seen that the size of the interparticle pores was around a few to tens of nanometers. The interstices between the AuAgNRs defined the permeability of CCs, selectively towards species smaller than the voids.^[5a,b,7] Different from individual AuAgNRs' optical absorption, intense broadband absorption was observed for CCs (Figure 1b). To provide mechanistic insight into this phenomenon, three-dimensional finite difference time domain (FDTD) analysis was performed to study the near-field distribution of electric field intensities in several simple assembly geometries (Figure S5) and a select area of CC surface of a real sample shown in Figure 1d (Figure 1g-i). From these calculation results, it could be deduced that the broadband absorption of the CCs was derived from an ensemble of the collective plasmonic near-field coupling effect between the adjacent AuAgNRs forming different assembly geometries in the microscale three-dimensional shell. Accordingly, the local electric fields are strongly enhanced at the "hot spots" around or in the gaps between the AuAgNRs over the whole surface of the CCs.

Then we integrated the CCs with bacteriorhodopsins by coating PM patches over the CC surfaces. PMs with ~ 5 nm in thickness and tens of nanometers to a few micrometers in width were isolated from *Halobacterium salinarum* strain S9 (Figure 2a-b). The peak around 570 nm in the UV-vis spectra could be assigned to the characteristic absorption of bacteriorhodopsin in its ground state (Figure 2c). The negatively charged nature of PMs enabled straightforward immobilization on positively charged CC surfaces via electrostatic interactions. As confirmed by zeta-potential measurements, the surface charge of CCs turned from positive to negative after coating with PMs (Figure S6). Notably, the presence of a film-like adherent layer on the surface in the SEM image (Figure 2d, 2e) provided direct evidence that the CCs were enveloped in PMs. It should be mentioned that no obvious damage of the CCs or PMs were observed during the wrapping process, highlighting their structural stability for further processing. Moreover, the presence of the absorption peaks at 280 and 570 nm in the UV-Vis spectrum (Figure 1f) and the increase in carbon content in the energy disperse X-ray analysis (Figure S7) further confirmed the successful coating of purple membranes. With a similar assembly process, we synthesized other types of protocells with CCs utilizing gold (Figure S8, AuNP) or SiO₂ nanoparticles (Figure S9, SiO₂NP) as building blocks, validating the generality of our method. By solubilizing bacteriorhodopsin from CC surfaces with detergent molecules of Triton X-100 (Figure S10), it was determined that about 19.6, 12.4 and 48.3 μg of bacteriorhodopsin assembled with 1 mg of AuAgNR, AuNP and SiO₂NP CCs, respectively.

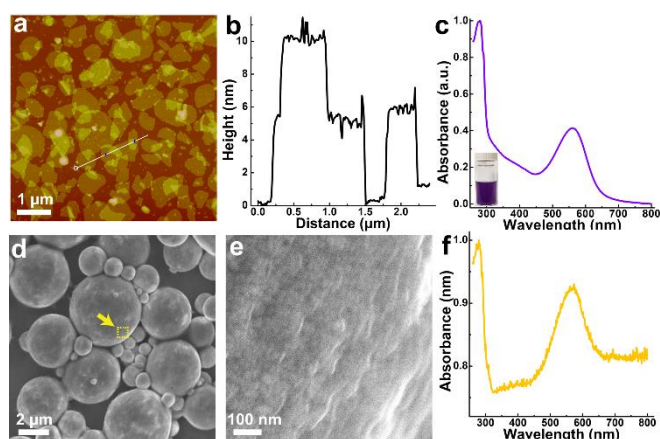


Figure 2. (a) Atomic force microscopy image, (b) height profile and (c) UV-vis absorption spectra of the PMs isolated from *H. salinarum*; inset in (c) is a suspension of purple membranes. (d) SEM image and (f) UV-vis absorption spectra of the purple membrane-coated CCs. (e) High-magnification SEM image of the arrow-pointed frame in (d).

Before studying the synthetic protocells' ability for photo-responsive proton pumping, their integrity was verified by dye release experiments. Negligible release of Rhodamine 110 was detected after 72 hrs in the solution containing intact synthetic protocells (Figure S11a). In contrast, >80% of the loaded dyes migrated across the protocell boundary within 30 mins after the introduction of Triton-X 100 (Figure S11b). Similar phenomena were also observed for cases with synthetic protocells using AuNP or SiO₂NP-stabilized CCs (Figure S12 and S13). These results suggested that owing to the rich positive sites on CC surfaces and the abundant negative charges on PMs, the resultant assembly was well sealed. The interior compartment of CCs was thus isolated from the surrounding solution, which would be important for forming a transmembrane gradient.^[12] Meanwhile, the quick passive diffusion of Rhodamine 110 (size < 1 nm) through 'peeled' protocells and the slight difference in release kinetics among the three kinds of CCs demonstrated the semi-permeability of the particle-packed shell towards substrates much smaller than the interstitial nanopores.^[6b, 7]

Next, photoinduced pH change in the suspension of synthetic protocells was monitored with a glass electrode attached to a pH meter. As shown in **Figure 3a** (red line), continuous illumination of the synthetic protocells with visible light (400 nm - 700 nm) provoked a decrease in pH of the external medium, indicating a net outward transport of protons. The pH change gradually reached a plateau value of about 0.52 units, which represented a steady state between the light driven forward proton movement and the back-pressure effect^[13] or passive proton permeation^[14]. After switching off the illumination, the pH variation slowly reversed, as protons passively diffused back^[14]. As controls, dark incubation, bare CCs, and CCs enveloped with apomembranes (bleached membranes, Figure S14) all led to negligible pH variation (**Figure 3b, i-iii**), suggesting that the bacteriorhodopsin functionality was well-preserved after fusion with CCs. Moreover, no acidification of the solution was detected for controls containing only free purple membrane fragments or a simple mixture AuAgNRs with purple membranes (**Figure 3b, iv-v**). The

latter fact indicates that CCs provided a framework for organizing a certain orientation of the PMs allowing for performing their biological function. In addition, proton uncouplers like carbonyl cyanide 3-chlorophenylhydrazone (CCCP) which increased the permeability of purple membranes for protons also abolished the light response (**Figure 3b, vi**). It should be mentioned that there was no detectable change in temperature of the solution during irradiation (Figure S15). Together, these results implied that by forming isolated compartmentalized configurations with CCs, bacteriorhodopsin could drive the transfer of protons across the membrane under irradiation, thereby allowing for the generation of a proton gradient.

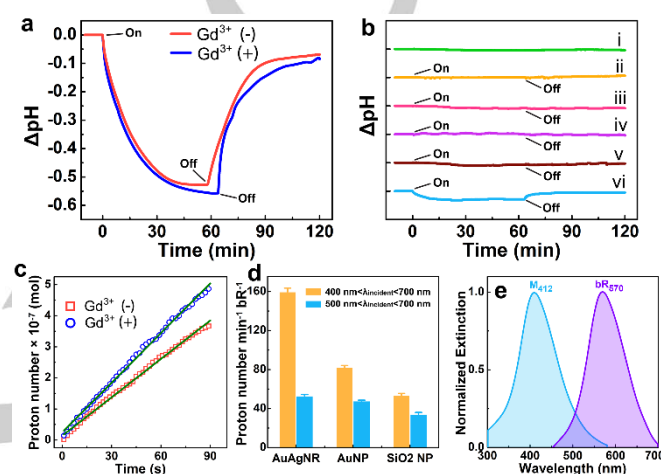


Figure 3. Light-induced variation of pH in the external medium of AgAuNR synthetic protocells (a) in the presence (+) and absence (-) of 5 μM Gd³⁺, and control groups (b). In panel b, one division of the y axis equals 0.1 pH unit and the plots were the pH changes in solutions of (i) synthetic protocells under dark conditions, (ii) bare CCs, (iii) control synthetic protocells made with apomembranes, (iv) free purple membranes, (v) simple mixture of AuAgNRs and purple membranes, and (vi) synthetic protocells in the presence of 10 μM protonophore CCCP; "On" and "Off" indicated the onset and offset of light irradiation, respectively. (c) The initial proton concentration changes in the presence and absence of Gd³⁺. (d) Proton pumping activities of bR in AgAuNR, AuNP and SiO₂NP synthetic protocells under light irradiation with different wavelengths. (e) The absorption spectra of M₄₁₂ and bR₅₇₀ intermediates.^[19b]

In its native state, transmembrane bacteriorhodopsin is asymmetrically oriented and pumps protons from the internal cytoplasm to the extracellular medium under illumination. Here the pH change suggested that most of the PM patches statistically biased right-side-out when assembled on the AuAgNR CC surface. This was presumably due to the intrinsic asymmetric charge distribution on the cytoplasmic and extracellular sides, which led to the preferential adhesion of one face onto positively charged surfaces.^[15] In the presence of Gd³⁺, we could see that the pH decrease was slightly faster and net pH change was slightly larger (**Figure 3a**, blue line). This was because lanthanide ions are non-permeant bacteriorhodopsin inhibitors only binding the carboxyl-terminal side^[16] and hence those inside-out bacteriorhodopsins in the synthetic protocells were blocked. By calculating the initial rates of external proton concentration change in the presence and absence of Gd³⁺ (**Figure 3c**, Figure S16), it could be estimated that ~81.5% of the bacteriorhodopsin

COMMUNICATION

was right-side-out. Also, approximately similar orientation efficiency was measured for synthetic protocells built with AuNP (79.5%, Figure S17) and SiO₂NP CCs (78.7%, Figure S18), which might be due to that the nanoparticles in all of the three kinds of CCs were modified with the same cationic ligands.

To interpret the contribution of AuAgNRs' plasmonic field to the function of synthetic protocells, we firstly compared the proton pumping activities of bR in AuAgNR synthetic protocells with those in the other two synthetic protocells utilizing AuNP- and SiO₂NP-based CCs (Figure 3d). It can be seen that bR in AuAgNR protocells showed the highest proton transporting rate, which was about 1.9 and 2.7 times higher than those of AuNP and SiO₂NP synthetic protocells, respectively. Given the negligible difference in cargo release kinetics of the three CCs studied above (Figure S11-13) and the well-known accelerated migration of protons assisted by mobile buffer molecules^[17], the possibility that the proton diffusion was the rate-limiting factor could be excluded. Instead, the difference in proton pumping kinetics can be explained with the difference in their optical properties. The ability of plasmonic nanostructures to strongly localize incident light close to their surface has been shown to greatly enhance the optical properties of proximal (bio-)molecules.^[18] The enhancement effect requires strong spectral overlap between the plasmonic resonance and (bio-)molecule absorption/emission band.^[18] In our case, AuAgNR CCs have a broad surface plasmon absorption (SPR) spectra that covered the entire visible range (Figure 1b), whereas AuNP CCs had strong SPR absorption only above 500 nm (Figure S8f) and SiO₂NP CCs had no SPR property at all (Figure S9f). On the other hand, bacteriorhodopsin has a series of spectrally distinguishable photocycle intermediates (Figure S1b), among which the two most important ground-state bR₅₇₀ and long-lived M₄₁₂ forms were studied in details because of their unique response to green and blue light irradiation, respectively. Excitation of bR₅₇₀ can induce the retinal isomerization to initiate the photocycle, while blue photons can speed up the reversal of the M₄₁₂ to the ground bR₅₇₀ by following the shorter bypass path (hundreds of ns) rather than the normal thermal decay (15 ms), known as the blue light effect (Figure S1b).^[19] With these in mind, it can be reasonably understood that the broad plasmon resonance of AuAgNR CCs overlapped well with the absorption contours of the bR₅₇₀ and M₄₁₂ intermediates (Figure 3e) and therefore could enhance the flux of photons at the corresponding wavelengths, thus increasing the probability of photoreactions. However, the SPR band of Au CCs only overlapped with bR₅₇₀, while SiO₂ CCs could do neither. Thus, the highest proton pumping rate was observed with AuAgNR synthetic protocells. This conclusion could be further supported by cutting off the blue light ($\lambda_{\text{incident}} > 500 \text{ nm}$, Figure 3d). In the absence of plasmon-enhanced blue light effect, AuAgNR synthetic protocells showed proton pumping rate comparable with AuNP synthetic protocells, but still higher than that of SiO₂NP synthetic protocells. Therein, the much larger decrease in magnitude associated with AuAgNR synthetic protocells also indicated that the plasmonic field effect and blue light effect collaboratively accelerated the kinetics of bacteriorhodopsin. As such, through mutually-enhancing fusion of stable semipermeable inorganic compartment with robust biological membrane proton pumping functionality, a new light-controllable synthetic protocell evolved.

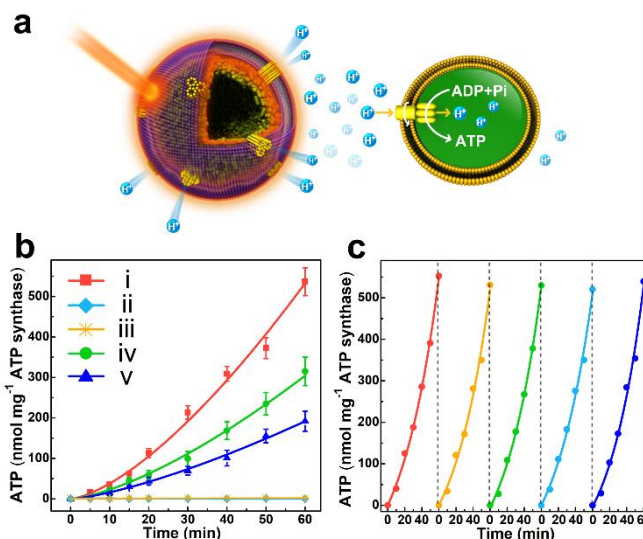


Figure 4. (a) Schematic illustration of the artificial communication process: light irradiation of AuAgNR synthetic protocells induced outward pumping of protons which were then transported by ATP synthase and triggered ATP synthesis in the second population of synthetic protocells (proteoliposomes). (b) ATP synthesis under different conditions: (i) AuAgNR synthetic protocells + proteoliposomes + light, (ii) AuAgNR synthetic protocells + proteoliposomes in dark, (iii) proteoliposomes + light, (iv) AuNP synthetic protocells + proteoliposomes + light, and (v) SiO₂NP synthetic protocells + proteoliposomes + light. (c) Recycled utilization of AuAgNR synthetic protocells for communicating with different batches of proteoliposomes for ATP synthesis.

Finally, we demonstrated the life-like potential of this system by studying its ability in communicating with another synthetic protocell population, where the outward-pumped protons acted as 'chemical signals' (Figure 4a). For benchmarking, ATP synthase-reconstituted liposomes (proteoliposomes) were introduced as the second population of protocells, since proton gradient could drive ATP synthase to catalyze the phosphorylation of ADP to ATP from in presence of inorganic phosphate by transporting protons across the enzyme^[20]. Chloroplast F₀F₁-ATP synthase was isolated and purified from spinach and then incorporated into liposomes (Figure S19, 20). The coexistence of two types of synthetic protocells in solution did not show much effect on the light-induced pH change of the external medium (Figure S21). Figure 4b-i showed that the ATP production continuously increased over the reaction time under illumination and yielded ca. 540 nmol ATP per mg of ATP synthase at 1 h. In contrast, no ATP was produced in the dark or in the absence of AuAgNR synthetic protocells under light irradiation (Figure 4b, ii-iii). These results confirmed that the outward protons pumped by the AuAgNR synthetic protocells led to the formation of proton gradient between the bulk solution and the interior space of the ATP synthase-incorporated synthetic protocells and thereby triggered the generation of ATP molecules. Meanwhile, lower ATP production rates were observed for synthetic communities using AuNP or SiO₂NP synthetic protocells (Figure 4b, iv-v). This could be due to that the initial rate of ATP synthesis relied on the magnitude of proton gradient,^[21] highlighting the contribution of the plasmonic resonance to the performance of the artificial system. Moreover, after separation and rebalance with buffer solution at the end of each cycle, AuAgNR synthetic protocells

can be reused to communicate with at least five batches of proteliposomes for triggering ATP synthesis with no obvious reduced performance (Figure 4c). Given that ATP is regarded as the energy currency of biological systems, here the coupling CC-based synthetic protocells with another population of synthetic protocells provided a sustainable solar-to-chemical energy conversion system.

In conclusion, we have successfully developed a light-gated synthetic protocell built with plasmonic colloidal capsules and bacteriorhodopsin for solar-to-proton gradient conversion and chemical communication-driven ATP synthesis. With this system, we investigated the effect of the plasmonic resonance of colloidal particles on boosting the proton pumping kinetics of the synthetic protocells. From a broader perspective, protocell models with similar designs using inorganic colloidal particles with different physicochemical (e.g. optical, catalytic, magnetic, electric, etc.) properties that have closer relevance to prebiotic chemistry would be instructive to decipher the roles inorganic matters played during the life evolution course. This protocell model also provides clues for directed evolution of cell-mimic functional materials with components more intimately engaged and augmenting one another. Furthermore, leveraging light to energize synthetic cells and activate signaling pathways represents a new paradigm for controlling prebiotic collective behaviors in a noninvasive and spatiotemporally precise manner, which may not be limited to complex synthetic communities and can be extended to interfacing with natural cells.

Acknowledgements

This material is based upon work supported by Laboratory Directed Research and Development (LDRD) and use of the Center for Nanoscale Materials was supported by the U.S. Department of Energy, Office of Science, Office of Basic Energy Sciences, under contract no. DE-AC02-06CH11357.

Keywords: protocell • colloidal capsule • bacteriorhodopsin • plasmonic resonance • chemiosmotic gradient

- [1] a) B. C. Buddingh', J. C. M. van Hest, *Acc. Chem. Res.* **2017**, *50*, 769-777; b) J. W. Szostak, *Angew. Chem. Int. Ed.* **2017**, *56*, 11037-11043; c) Z. Chen, J. Wang, W. Sun, E. Archibong, A. R. Kahkoska, X. Zhang, Y. Lu, F. S. Ligler, J. B. Buse, Z. Gu, *Nat. Chem. Biol.* **2018**, *14*, 86-93; d) T. Trantidou, M. Friddin, Y. Elani, N. J. Brooks, R. V. Law, J. M. Seddon, O. Ces, *ACS Nano* **2017**, *11*, 6549-6565; e) Q. Zou, L. Zhang, X. Yan, A. Wang, G. Ma, J. Li, H. Möhwald, S. Mann, *Angew. Chem. Int. Ed.* **2014**, *53*, 2366-2370.
- [2] a) J. Lombard, P. López-García, D. Moreira, *Nat. Rev. Microbiol.* **2012**, *10*, 507; b) M. M. Hanczyc, S. M. Fujikawa, J. W. Szostak, *Science* **2003**, *302*, 618-622; c) N.-N. Deng, W. T. S. Huck, *Angew. Chem. Int. Ed.* **2017**, *56*, 9736-9740.
- [3] a) W. Martin, J. Baross, D. Kelley, M. J. Russell, *Nat. Rev. Microbiol.* **2008**, *6*, 805; b) E. V. Koonin, W. Martin, *Trends Genet.* **2005**, *21*, 647-654; c) N. Lane, William F. Martin, *Cell* **2012**, *151*, 1406-1416.
- [4] M. Li, X. Huang, T. Y. D. Tang, S. Mann, *Curr. Opin. Chem. Biol.* **2014**, *22*, 1-11.
- [5] a) T. Bollhorst, K. Rezwan, M. Maas, *Chem. Soc. Rev.* **2017**, *46*, 2091-2126; b) A. D. Dinsmore, M. F. Hsu, M. G. Nikolaidis, M. Marquez, A. R. Bausch, D. A. Weitz, *Science* **2002**, *298*, 1006-1009; c) D. Liu, F. Zhou, C. Li, T. Zhang, H. Zhang, W. Cai, Y. Li, *Angew. Chem. Int. Ed.* **2015**, *54*, 9596-9600; d) G. C. Phan-Quang, H. K. Lee, I. Y. Phang, X. Y. Ling, *Angew. Chem. Int. Ed.* **2015**, *54*, 9691-9695.
- [6] M. Li, D. C. Green, J. L. R. Anderson, B. P. Binks, S. Mann, *Chem. Sci.* **2011**, *2*, 1739-1745.
- [7] M. Li, R. L. Harbron, J. V. Weaver, B. P. Binks, S. Mann, *Nat. Chem.* **2013**, *5*, 529-536.
- [8] M. Li, X. Huang, S. Mann, *Small* **2014**, *10*, 3291-3298.
- [9] a) L. Rodríguez-Arco, M. Li, S. Mann, *Nat. Mater.* **2017**, *16*, 857; b) S. Sun, M. Li, F. Dong, S. Wang, L. Tian, S. Mann, *Small* **2016**, *12*, 1920-1927.
- [10] a) N. Hampp, *Chem. Rev.* **2000**, *100*, 1755-1776; b) P. Wang, A. Y. Chang, V. Novosad, V. V. Chupin, R. D. Schaller, E. A. Rozhkova, *ACS Nano* **2017**, *11*, 6739-6745; c) S. Balasubramanian, P. Wang, R. D. Schaller, T. Rajh, E. A. Rozhkova, *Nano Lett.* **2013**, *13*, 3365-3371.
- [11] a) K. Stratford, R. Adhikari, I. Pagonabarraga, J.-C. Desplat, M. E. Cates, *Science* **2005**, *309*, 2198-2201; b) Y. Lin, H. Skaff, T. Emrick, A. D. Dinsmore, T. P. Russell, *Science* **2003**, *299*, 226-229; c) Z. Chen, L. Zhou, W. Bing, Z. Zhang, Z. Li, J. Ren, X. Qu, *J. Am. Chem. Soc.* **2014**, *136*, 7498-7504; d) Z. Chen, H. Ji, C. Zhao, E. Ju, J. Ren, X. Qu, *Angew. Chem. Int. Ed.* **2015**, *54*, 4904-4908; e) A. Kulak, S. A. Davis, E. Dujardin, S. Mann, *Chem. Mater.* **2003**, *15*, 528-535.
- [12] G. Nordlund, J. B. Sing Ng, L. Bergström, P. Brzezinski, *ACS Nano* **2009**, *3*, 2639-2646.
- [13] N. Calimet, G. Matthias Ullmann, *J. Mol. Biol.* **2004**, *339*, 571-589.
- [14] M. Seigneuret, J. L. Rigaud, *Biochemistry* **1986**, *25*, 6716-6722.
- [15] a) K. Fisher, K. Yanagimoto, W. Stoeckenius, *J. Cell. Biol.* **1978**, *77*, 611-621; b) J.-A. He, L. Samuelson, L. Li, J. Kumar, S. K. Tripathy, *Langmuir* **1998**, *14*, 1674-1679; K. M. Bromley, A. J. Patil, A. M. Seddon, P. Booth, S. Mann, *Adv. Mater.* **2007**, *19*, 2433-2438.
- [16] J. L. Rigaud, M. T. Paternostre, A. Bluzat, *Biochemistry* **1988**, *27*, 2677-2688.
- [17] V. A. Lorenz-Fonfria, M. Saita, T. Lazarova, R. Schlesinger, J. Heberle, *Proc. Natl. Acad. Sci. USA* **2017**, *114*, E10909-E10918.
- [18] a) I. Kim, S. L. Bender, J. Hranisavljevic, L. M. Utschig, L. Huang, G. P. Wiederrecht, D. M. Tiede, *Nano Lett.* **2011**, *11*, 3091-3098; b) R. Zhang, Y. Zhang, Z. C. Dong, S. Jiang, C. Zhang, L. G. Chen, L. Zhang, Y. Liao, J. Aizpurua, Y. Luo, J. L. Yang, J. G. Hou, *Nature* **2013**, *498*, 82; c) Y. Chen, K. Munechika, D. S. Ginger, *Nano Lett.* **2007**, *7*, 690-696.
- [19] a) B. Hessling, J. Herbst, R. Rammelsberg, K. Gerwert, *Biophys. J.* **1997**, *73*, 2071-2080; b) L.-K. Chu, C.-W. Yen, M. A. El-Sayed, *J. Phys. Chem. C* **2010**, *114*, 15358-15363; c) C.-W. Yen, L.-K. Chu, M. A. El-Sayed, *J. Am. Chem. Soc.* **2010**, *132*, 7250-7251.
- [20] Y. Li, J. Fei, G. Li, H. Xie, Y. Yang, J. Li, Y. Xu, B. Sun, J. Xia, X. Fu, J. Li, *ACS Nano* **2018**, *12*, 1455-1461.
- [21] Q. He, L. Duan, W. Qi, K. Wang, Y. Cui, X. Yan, J. Li, *Adv. Mater.* **2008**, *20*, 2933-2937.

COMMUNICATION

Entry for the Table of Contents (Please choose one layout)

Layout 1:

COMMUNICATION

Text for Table of Contents

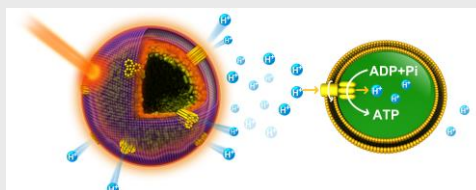
Author(s), Corresponding Author(s)*

Page No. – Page No.

Title

Layout 2:

COMMUNICATION



Light-gated synthetic protocells were built with plasmonic colloidal capsules and bacteriorhodopsin for solar-driven proton gradient generation and communication-mediated ATP synthesis, where the impact of colloidal particles' plasmon resonance on the performance of the cytomimetic system was studied.

Z. Chen, G. De Queiros Silveira, X. Ma, Y. Xie, Y. A. Wu, E. Barry, T. Rajh, H. C. Fry, P. D. Laible, E. A. Rozhkova*

Page No. – Page No.

Light-Gated Synthetic Protocells for Plasmon-Enhanced Chemiosmotic Gradient Generation and Phosphorylation